Modelling and characterisation of Mo_2C precipitation and cementite dissolution during tempering of Fe–C–Mo martensitic steel

S. Yamasaki and H. K. D. H. Bhadeshia

The precipitation and Ostwald ripening behaviour of needle shaped Mo_2C particles during the tempering of a ternary Fe–C–Mo martensitic steel have been characterised and modelled, taking account of local equilibrium, the capillarity effect, and the simultaneous enrichment and dissolution of cementite. Particles of Mo_2C are represented as paraboloids of revolution, with the tip radius chosen to yield the maximum lengthening rate. Transmission electron microscopy has been used to validate the theory; measurements of the average length, volume fraction, and number density of particles showed good agreement with experimental observations. MST/5585

At the time the work was carried out the authors were in the Department of Materials Science and Metallurgy, University of Cambridge, Pembroke Street, Cambridge CB2 3QZ, UK (hkdb@cus.cam.ac.uk). Mr Yamasaki (yamasaki@to.kimitsu.nsc.co.jp) is now with Nippon Steel Corp., 1 Kimitsu, Kimitsu City, 299–1141 Japan. *Manuscript received 15 July 2002; accepted 15 July 2002.*

List of symbols

a	activity
$c^{\alpha\beta}_{Mo}$	atomic fraction of molybdenum in α in equilibrium with β
$c^{\alpha\beta}_{Mo,r}$	atomic fraction of molybdenum in α in equilibrium with β at a curved interface
c^{θ}_{Mo}	atomic fraction of molybdenum in θ
$\bar{c}_{Mo}$	atomic fraction of molybdenum in the alloy
$\bar{d}$	mean diffusion distance between precipitates
d_t	thickness of a cementite particle
D_{Mo}	diffusion coefficient of molybdenum
G^*	activation energy for nucleation
h	Planck constant
H	curvature of a particle
H^{SER}	enthalpy of the element or substance in the reference state at 25·15°C
I	nucleation rate
k	Boltzmann constant
N	number density of nucleation sites
N_A	Avogadro's number
N^{β}	number density of β precipitates
N^{β}_0	initial number density of β precipitates of the Ostwald ripening stage
P	pressure
$\bar{p}$	Péclet number
Q^*	activation energy for the transfer of atoms across the interface
r_c	critical tip radius at which growth ceases
r^{TC}	radius of curvature at the tip
r^*	nucleus size
r_0	initial average particle radius of the Ostwald ripening stage
T	absolute temperature
t	time
v	growth rate of a particle
v_c	growth rate of a flat interface governed by the interface process
Γ	capillarity coefficient
ζ_θ	volume fraction of θ phase
μ^{α}_X	chemical potential per X atom in α
μ^{β}_X	chemical potential per X atom in β
v^{β}	volume of an atom in β phase
σ	interfacial energy per unit area
Ω	supersaturation

Introduction

Alloy carbides have played an important role in the development of structural steels, for example, in the strengthening and toughening of microalloyed steels and in the exploitation of secondary hardened steels for service at elevated temperatures. A less well known application is when carbides, such as Mo_2C and V_4C_3 are introduced into the steel as hydrogen trapping sites to enhance the resistance to static fracture of components such as springs, bolts and power plant items;[1,2] it is in this context that the present work was initiated.

The mechanical and hydrogen trapping properties depend on many parameters but the two most significant terms are the carbide size and number density. These parameters have in the past been manipulated on the basis of experience and experimental work. The aim in this research was to develop a model for estimating the kinetics of alloy–carbide microstructures during the tempering of steels, in the hope of accelerating the design process for novel, hydrogen resistant steels.

Fujita and Bhadeshia modelled the precipitation of Mo_2C accounting approximately for the capillarity effect in a ternary system.[3] The carbide particles were assumed to be in the form of thin cylinders with hemispherical ends, as in the Zener treatment.[4] A disadvantage of their method is that the needle aspect ratio had to be chosen arbitrarily. The purpose of the present work was to improve on that model, with a better representation of the shape of the precipitate and to simulate the tempering of a Fe–C–Mo ternary martensitic steel. The work is based on Trivedi's solution[5] for the growth of paraboloids of revolution, and local equilibrium, the capillarity effect, and simultaneous cementite enrichment and dissolution in a multicomponent system are accounted for in this paper.

PRECIPITATION OF ALLOY CARBIDE WITH LOCAL EQUILIBRIUM

Carbon is an interstitial solute in iron and hence has a much higher mobility than substitutional solutes or iron. It is natural therefore that iron carbides are the first to form

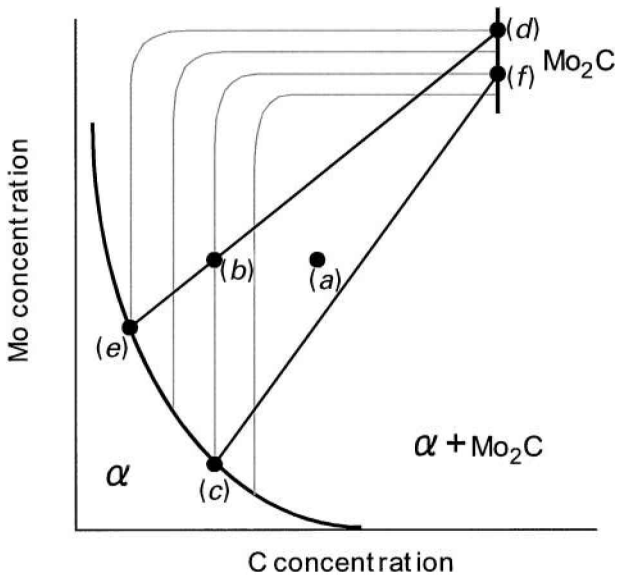

1 Schematic representation of alloy composition and tie lines governing α/Mo_2C interface compositions during precipitation process: point (a) is alloy composition and (b) is matrix composition after paraequilibrium cementite precipitation; points (c) and (f) are both ends of interface composition contour passing through point (b), which are α/Mo_2C interface compositions

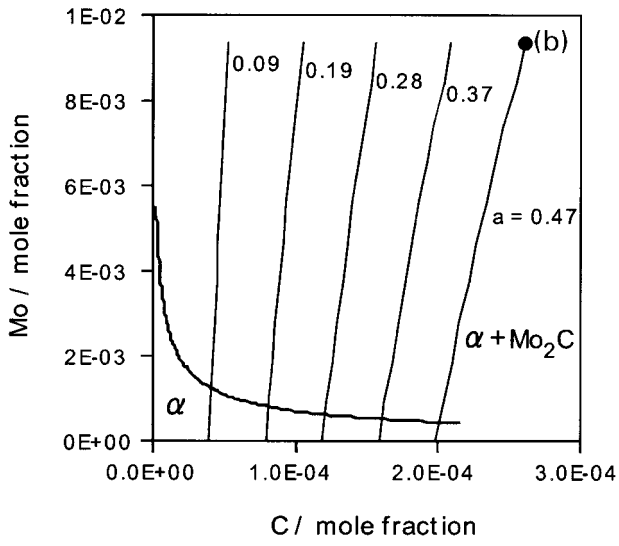

2 Several isoactivity curves for carbon in $\alpha + Mo_2C$ two phase field: values in figure designate activity *a* of carbon; point (b) represents ferrite composition after completion of paraequilibrium precipitation

when virgin martensite is tempered. In low and medium carbon steels containing dislocated martensite, cementite precipitates first in the tempering process. This cementite grows by a paraequilibrium mechanism; paraequilibrium is a state in which carbon achieves a uniform chemical potential across the interface subject to the constraint that the substitutional solute to iron atom ratio is maintained constant everywhere.[6] Thus, paraequilibrium cementite seems to form by a displacive mechanism.[7–10]

The steps following the rapid precipitation of paraequilibrium cementite are complicated because its chemical composition changes towards equilibrium because cementite absorbs molybdenum (enriches) as it tries to achieve its equilibrium composition. Cementite, although kinetically favoured, is less stable than many alloy carbides; consequently, while the cementite adapts its chemical composition, molybdenum carbide precipitation commences and eventually leads to the dissolution of the cementite. These processes must all be considered to occur simultaneously in any model.

In the present case, alloy carbide formation involves the diffusion of both molybdenum and carbon, the diffusivities of which are different by many orders of magnitude at the transformation temperature. In order to maintain equilibrium at the transformation interface, the tie line controlling interface compositions has to be chosen in such a way that the two solutes can keep pace with each other.[11] Another way of expressing this condition is to construct interface composition (IC) contours on isothermal sections of the ternary phase diagram; all alloys on this contour transform with the same compositions (same tie line) at the interface, whilst ensuring that the slow and fast solute diffusion fluxes are both consistent with the rate at which the interface moves. The IC contour depends on the ratio of the diffusion coefficients of the substitutional solute X and of carbon D_X/D_C.

Considering this scenario, the precipitation process in a ternary alloy can be illustrated by Fig. 1. Point (a) is the overall composition of the alloy, i.e. the composition of the virgin martensite. Point (b) is the matrix composition after paraequilibrium cementite precipitation; this matrix is supersaturated with respect to molybdenum carbide, which will precipitate with the interface compositions given by the tie line (c)–(f). As it continues to precipitate, the less stable cementite dissolves; this effectively moves (b) in a direction such that the governing tie line shifts from (c)–(f) towards (e)–(d). This tie line shifting[11] ceases when the governing tie line passes through the average composition (a) and equilibrium is achieved. The cementite acts as a source of carbon.

In Fig. 1, to satisfy the mass balances of Mo and C, the interfacial C concentration is assumed to be the same as that of the matrix.[11] However, it is strictly not the C concentration but the activity of C which should be identical for the ferrite/Mo_2C interface and in the matrix far from the interface. If the interaction between substitutional atoms is strong, e.g. for the case of C and Cr, the above assumption is not strictly valid. Figure 2 shows several isoactivity curves in the $\alpha + Mo_2C$ two phase field. As shown in Fig. 2, the deviation of the isoactivity curves from the isocarbon concentration lines (the perpendicular lines) is small and the assumption in Fig. 1 is therefore considered to be valid.

GROWTH OF PARTICLES: CAPILLARITY

There is a variety of models dealing with the diffusion controlled growth of needle shaped particles.[4,5,12,13] Amongst them, the most comprehensive theory is due to Trivedi,[5] following work by Ivantsov,[12] in which a needle shaped particle is represented as a shape preserving paraboloid of revolution. The curvature is not therefore constant across the surface of the needle; Trivedi therefore introduced the functions R_1 and R_2 to account for capillarity and interface kinetics respectively, over the surface of the paraboloid

$$\Omega = \bar{p}\exp(\bar{p})E_1(\bar{p})\left[1+\frac{v}{v_c}\,\Omega R_1(\bar{p})+\frac{r_c}{r^{IC}}\,\Omega R_2(\bar{p})\right] \qquad (1)$$

where Ω is the supersaturation, r^{IC} is the radius of curvature at the tip, r_c is the critical tip radius at which growth ceases, v is the lengthening rate, v_c is the velocity of a flat interface which is completely controlled by the interface processes, $\bar{p}$ is the Péclet number ($\bar{p} = vr^{IC}/2D$) and $E_1(\bar{p})$ represents the exponential integral.[14] The values of $R_1(\bar{p})$ and $R_2(\bar{p})$ are

$$\left.\begin{aligned} R_1(\bar{p}) &= (2\bar{p})^{-1}N_1(\bar{p})-1 \\ R_2(\bar{p}) &= (4\bar{p})^{-1}N_2(\bar{p})-1 \end{aligned}\right\} \qquad (2)$$

The values of functions $N_1(\bar{p})$ and $N_2(\bar{p})$ were obtained numerically by Trivedi and they become 1·4050 and 3·8410

for small values of supersaturation ($\Omega \ll 1$), respectively.[5] Equation (1) gives the general solution for the growth of precipitate needles. The right hand side is a sum of three terms of which the first is the result obtained by Ivantsov[12] for the case of the isoconcentrate boundary. The second and the third terms are corrections to that solution owing to the interface kinetics and capillarity effects respectively.

Equation (1) yields the Péclet number as a function of the supersaturation, but a further assumption is needed to obtain a lengthening rate or tip radius. Zener suggested that the particle should adopt a tip radius which gives the maximum growth rate.[4] This maximum growth rate can be obtained by differentiating equation (1) with respect to r^{IC} and setting $\partial v/\partial r^{IC} = 0$. The solution of the differential was obtained for large values of Ω ($\Omega \geqslant 0{\cdot}2$)[15] and for small values of $\Omega \leqslant 0{\cdot}2$.[16] In the present work, diffusion controlled growth was assumed; the kinetics term in equation (1) was therefore neglected.

Experimental work

Experiments were conducted to provide data for model verification. As shown later, the model can predict the average carbide length, volume fraction and number density. It is therefore necessary to obtain these data experimentally to verify the model. The necessary data was obtained using TEM.

MATERIAL

The chemical composition of the material designed for the present work was: Fe–0·10C–<0005Si–1·99Mn–1·60Mo–0·03Al–0·0049N (wt-%). The steel contains 0·1 wt-% carbon and a stoichiometric quantity of molybdenum for Mo_2C. As will be shown later, experimental data and thermodynamic calculations show that in this steel the carbide is virtually pure Mo_2C with negligible quantities of iron or manganese in the metal sites. Therefore, its precipitation is modelled as if it occurs in a ternary Fe–C–Mo system.

The steel was vacuum melted as a 10 kg ingot, heated at 1250°C for 30 min in an argon atmosphere, hot rolled to 12 mm thickness plate and air cooled. From this plate, the specimens for heat treatment were machined to 3 and 8 mm diameter. The specimens were sealed in silica tubes under a partial pressure of argon (~150 mm Hg), before normalising. According to equilibrium calculation using MTDATA, the steel should be fully austenitic at temperatures above 1000°C. The homogenisation temperature was therefore chosen to be 1250°C, at which the specimens were held for 50 h.

After the homogenisation treatment, the specimens were quenched into water and the silica tubes were broken. Then, specimens were sealed again and tempered at 600°C from 0·5–1160 h. After tempering, all specimens were again quenched into water, breaking the silica tube.

SPECIMEN PREPARATION

Two types of specimens were examined using TEM: thin foils and carbon extraction replicas. Thin foil observation is crucial to define the orientation relationship between the precipitates and the matrix. Thin foils were sliced from bulk specimens as 3 mm diameter discs to ~250 μm thickness using a silicon carbide blade and cooling lubricant. After slicing, the specimens were ground with silicon carbide paper to around 50 μm thickness. Electropolishing was conducted using a twin jet electropolisher.[17] The solutions used for electropolishing were 5 vol.-% perchloric acid, 20 vol.-% glycerol and 75 vol.-% methanol. The electropolishing was performed with the solution at 15°C, the electrical potential being set at 50 V.

Carbon replica (single stage extraction) specimens were also prepared from each specimen. Specimens with 8 mm diameter were hot mounted with Bakelite moulding powder, and ground with silicon carbide paper down to 1200 grit and then polished with 6 and 1 μm diamond pastes. They were then chemically etched with 4 vol.-% nital for a few seconds. A carbon coating of 20–30 nm (brown gold color) was deposited in a vacuum of 10^5 torr (133 322 mbar) onto the etched surface. This film was then scored with a sharp blade to divide it into several smaller squares (~1 mm^2). Electrolytic etching in a solution of 5 vol.-% hydrochloric acid in methanol at 7·5 V was used to remove the carbon film, which was then washed in methanol and floated off in distilled water. These films were mounted on copper grids.

TEM OBSERVATION

Molybdenum carbide

Figure 3 shows thin foil TEM images of the specimens tempered for a variety of times. These pictures were taken from the [001] orientation of the ferritic matrix. Figure 4 shows TEM images of a carbon replica specimen from the steel tempered for 560 h. From the diffraction patterns in Fig. 4, the needle shaped precipitates have a hexagonal close packed (hcp) structure and are considered to be M_2C, where M stands for metal atoms (Mo, Mn, Fe). The chemical compositions of M_2C particles were measured using energy dispersive spectroscopy using carbon replica specimens; the average ratio of metallic elements is 0·91Mo : 0·06Mn : 0·02Fe. These precipitates are therefore virtually pure Mo_2C. It is known that Mo_2C grows along the three equivalent $\langle 001 \rangle_\alpha$ directions, and, for example in Fig. 3, precipitates growing in three $\langle 001 \rangle_\alpha$ directions are observed. In Fig. 3, the point like precipitates are the cross-section images of precipitates growing in the [001] direction, which is parallel to the observation direction.

Foil thickness

A knowledge of the thickness of the foils used for TEM is necessary to estimate the volume fraction of Mo_2C. It was calculated using thickness fringes at the grain boundaries. The extinction distances for a two beam condition are known; it is therefore possible to calculate the thickness of the specimen by multiplying the extinction distance by the number of fringes. The thicknesses of the specimens were in this way found to be between 80 and 160 nm.

Cementite

Figure 5 shows an example of a carbon extraction replica TEM image of the steel tempered at 600°C for 10 h. Cementite particles precipitate on the prior austenite grain boundaries and the martensite lath boundaries. Cementite particles are also evident within the laths. Particles precipitating on the boundaries are spheroidal or plate shaped and the average thickness is 50 nm. On the other hand, the particles precipitating within the laths are plate shaped and the average thickness is 20 nm. Cementite in the laths dissolved after 100 h tempering at 600°C, but it persisted on the grain boundaries.

Carbide morphology and volume fraction

The Mo_2C grows at the expense of cementite. Mo_2C grows in the $\langle 001 \rangle_\alpha$ directions whilst keeping a needle shape whose average aspect ratio is about 9–10. The carbide size was measured for each specimen from at least five different locations, each of which contained over 300 particles. The volume fraction was calculated using the length and diameter of each carbide particle and the foil thickness. The average carbide length, volume fraction, number density and number density distribution of the length of Mo_2C particles are shown elsewhere in this paper along with the predictions made using the model (*see* Fig. 8).

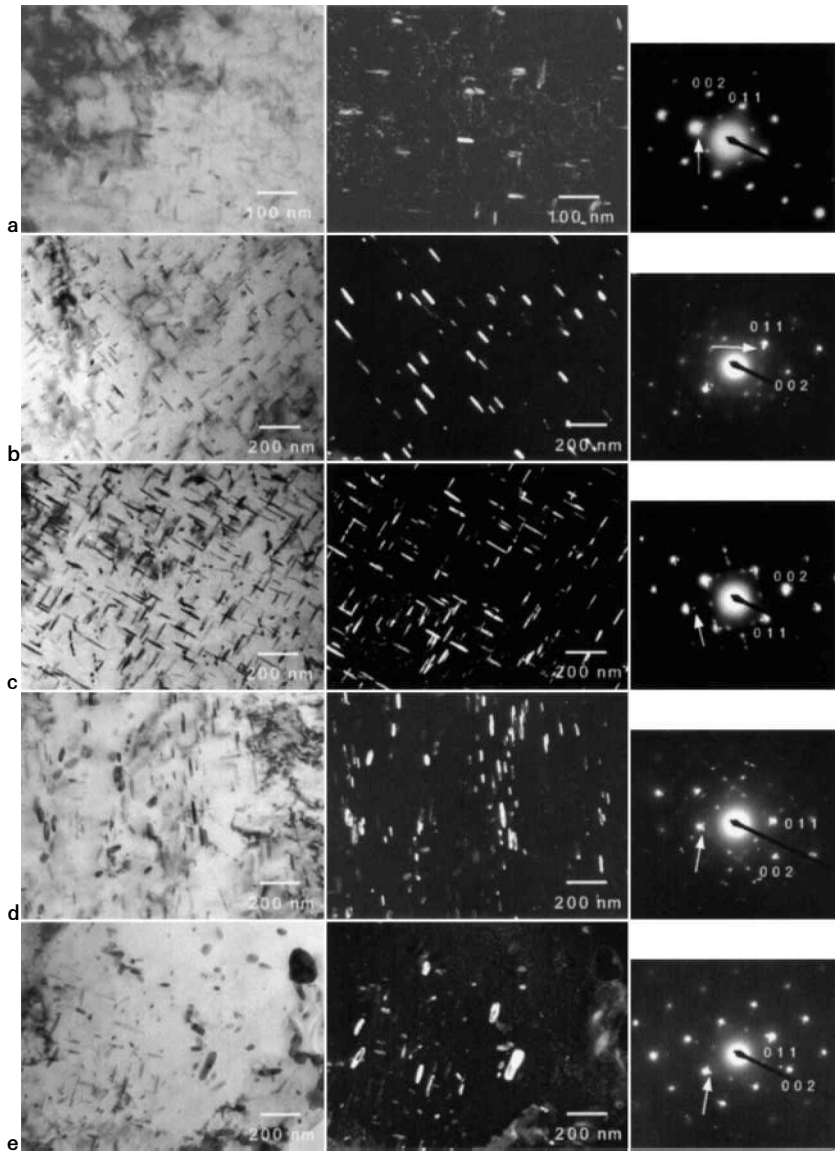

a 10 h; *b* 30 h; *c* 100 h; *d* 560 h; *e* 1160 h

3 Observation (TEM) of test steel tempered at 600°C for different times: zone axis is [001] of ferrite; each dark field image was taken using diffraction spot indicated by arrow

Modelling of needle shaped carbide growth

CHEMICAL COMPOSITION AND EQUILIBRIUM PHASES

Using MTDATA, the phase fractions and the compositions of the equilibrium carbides for the steel at a variety of temperatures were calculated. The calculations allowed for the potential existence of cementite, M_2C (hcp), MC (fcc), M_7C_3, M_6C and $M_{23}C_6$ in addition to ferrite. According to the results, for 600°C, M_2C (hcp) is the only stable carbide in this steel. The equilibrium composition of M_2C according to MTDATA is 0·57Mo–0·33C–0·09Mn–0·01Fe in mole fraction. It is therefore designated Mo_2C in a Fe–C–Mo ternary system.

CAPILLARITY EFFECT, MULTICOMPONENT SYSTEMS

When precipitates are curved the need to create new interfacial area affects local equilibrium, an effect which cannot be neglected when dealing with small particles or coarsening reactions. If α and a sphere of β are in contact at a curved interface then the conditions for local equilibrium are[18]

$$dT^{\beta} = dT^{\alpha} = dT \quad . . . . . (3)$$

$$dP^{\beta} = dP^{\alpha} + 2\sigma\, dH \quad . . . . . (4)$$

$$d\mu_1^{\beta} = d\mu_1^{\alpha}, \quad d\mu_2^{\beta} = d\mu_2^{\alpha} \quad . . . . . (5)$$

Here T, P, H, σ and μ represent temperature, pressure, curvature of β phase, surface energy, and chemical potential, respectively. If it is assumed that the pressure of the α phase is constant, from equation (4), the pressure change of the β phase can be represented as

$$\Delta P = \int_{P(H=0)}^{P} dP^{\beta} = \int_{H=0}^{H} 2\sigma\, dH = 2\sigma / r^{IC} \quad . . . . (6)$$

where r^{IC} is the radius of curvature at the tip. Accordingly, if the atomic volume of β is represented as v^{β}, the additional Gibbs energy term of ΔG^{β} is

$$\Delta G^{\beta} = \Delta P v^{\beta} = 2\sigma v^{\beta} / r^{IC} \quad . . . . . (7)$$

The simplest exact method to evaluate the influence of capillarity on the interface composition is to increase the

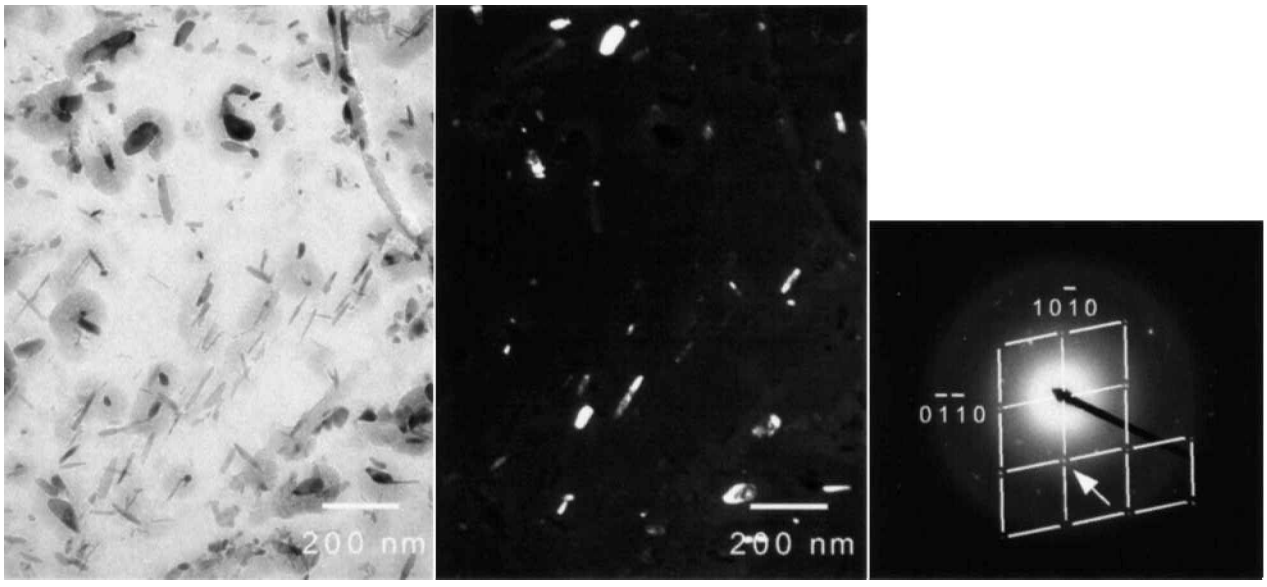

a b c

b is dark field image of diffraction spot indicated by arrow in *c*

4 Observation (TEM) of extraction carbon replica specimen from steel tempered at 600°C for 560 h: precipitates are M_2C

Gibbs energy of the β phase in the database used by thermodynamic calculation software such as MTDATA.[19] In MTDATA, the free energy of a phase such as ferrite is calculated using a sublattice model which involves terms called unaries. Commonly, the temperature and pressure dependence of unaries are described using the G-HSER format

$$G^{T,P} - H^{SER} = a + bT + cT\ln T + eT^2 + fT^3 + i/T + \int_0^P v^{P,T} N_A \, dP \quad \ldots\ldots\ldots (8)$$

where $G^{T,P}$ is the molar Gibbs energy at (T, P), $v^{T,P}$ is the atomic volume at (T, P), N_A is Avogadro's number and H^{SER} is the enthalpy of the element or substance in the reference state at 298·15 K (25·15°C). Although the data contained in the SGTE solutions and substances database do not include pressure dependent terms for most phases, it is possible to modify the database to add such terms. For example, in case of Mo_2C (hcp, $a = 0{\cdot}3$ nm, $c = 0{\cdot}472$ nm), the atomic volume v^{Mo_2C} is $1{\cdot}22 \times 10^{-29}$ m^3 and interfacial energy σ can be assumed 0·2 J m^{-2} (Ref. 20), and accordingly, the additional Gibbs energy would be 2941 J mol^{-1} for $r^{IC} = 1$ nm. The database of the hcp phase (sublattice) was modified to add 1×10^{-6} J mol^{-1} per 1 Pa pressure increase.

The effect of capillarity on the molybdenum concentration in the ferrite which is in local equilibrium with the carbide $c^{\alpha Mo_2C}_{Mo,r}$ evaluated by increasing an additional Gibbs energy term in the database of MTDATA, is shown in Fig. 6 as a function of the radius of curvature, for 0·1C–1·60Mo (wt-%) steel.

OVERALL TRANSFORMATION KINETICS

The carbide reaction during tempering in a Fe–C–Mo steel, which includes the precipitation of Mo_2C, and the enrichment and dissolution of cementite, was simulated.

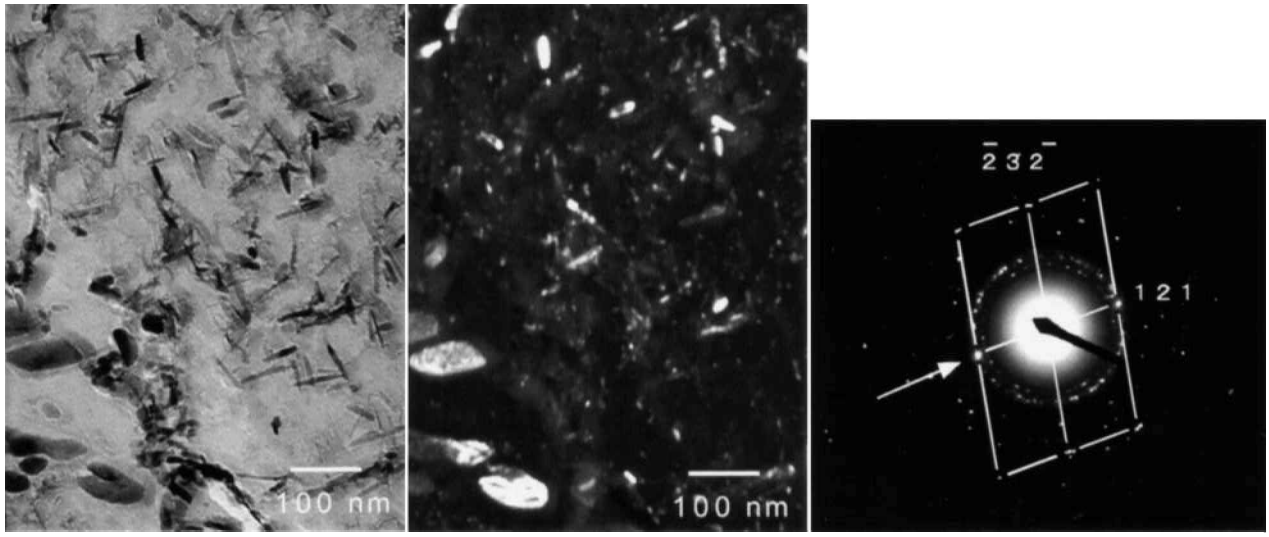

a b c

b is dark field image of diffraction spot indicated by arrow in *c*

5 Observation (TEM) of extraction carbon replica specimen from steel tempered at 600°C for 10 h: precipitates are cementite

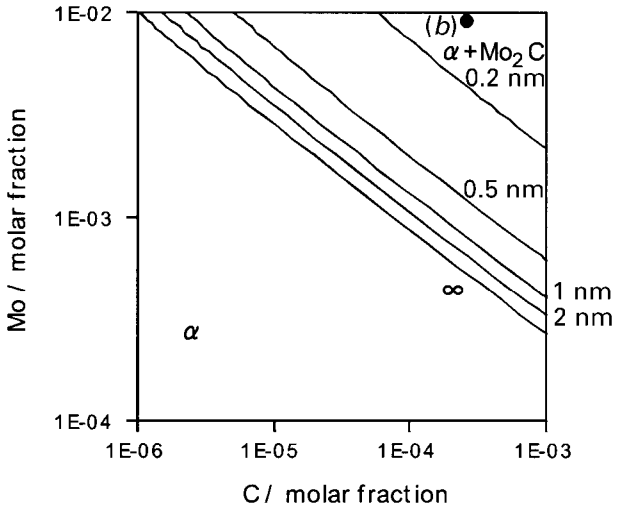

6 Capillarity corrected composition of ferrite in equilibrium with Mo_2C as function of radius of curvature: point (b) designates composition of ferrite matrix after completion of paraequilibrium cementite precipitation

Enrichment and dissolution of cementite

Cementite is assumed initially to contain a molybdenum to iron atom ratio as in the average chemical composition. During tempering, molybdenum diffuses into the cementite to enrich it towards equilibrium, and at some stage, the cementite begins to dissolve to give way to the precipitation of the more stable Mo_2C. The volume fraction of cementite can be calculated using the lever rule and assuming that any residual carbon concentration in the ferrite is so small that can be neglected. The volume fraction of cementite ζ_θ is then given by[21]

$$\xi_\theta = 1{\cdot}0065 \times \bar{c}/c^{\theta\alpha} \quad c^{\theta\alpha} \approx 0{\cdot}25 \quad . \quad . \quad . \quad . \quad . \quad . \quad . \quad (9)$$

by taking account of the difference in ferrite and cementite densities. As indicated by TEM, there was an average cementite plate thickness of $\sim 2 \times 10^{-8}$ m when the particles were within the ferrite grains and 5×10^{-8} m when on the grain boundaries.

The rate of enrichment is given approximately by[22]

$$c^{\theta}_{Mo} = \bar{c}_{Mo} + 4(D_{Mo}t)^{1/2}(\bar{c}_{Mo} - c^{\alpha\theta}_{Mo})/(d_t\pi^{1/2}) \quad . \quad . \quad . \quad (10)$$

where c^{θ}_{Mo} represents the atomic fraction of Mo in cementite, t is the time since cementite formation, d_t is the thickness of the cementite plate, D_{Mo} is the diffusion coefficient of Mo in the matrix (it is assumed that the corresponding diffusivity in the cementite is identical to that in ferrite), $c^{\alpha\theta}_{Mo}$ is the atomic fraction of Mo in the ferrite which is in equilibrium with the cementite, and $\bar{c}_{Mo}$ is the mean atomic fraction of Mo in the alloy.

The dissolution rate v_θ is determined as[23]

$$v_\theta = -\frac{D_{Mo}}{d}\frac{c^{\alpha\theta}_{Mo} - c^{\alpha Mo_2C}_{Mo}}{c^{\theta\alpha}_{Mo} - c^{\alpha\theta}_{Mo}} \quad . \quad . \quad . \quad . \quad . \quad . \quad . \quad . \quad (11)$$

where $\bar{d}$ is the mean diffusion distance between θ and Mo_2C precipitates, given by

$$\bar{d} = (N^\theta + N^{Mo_2C})^{-1/3} \quad . \quad . \quad . \quad . \quad . \quad . \quad . \quad . \quad . \quad (12)$$

where N^θ and N^{Mo_2C} are the number densities of θ and Mo_2C particles respectively.

Nucleation of Mo_2C

The nucleation rate of Mo_2C particles is given as

$$I = N\frac{kT}{h}\exp\left[\frac{-(G^* + Q^*)}{kT}\right] \quad . \quad . \quad . \quad . \quad . \quad . \quad . \quad (13)$$

where N is the number density of nucleation sites, Q^* is the activation energy for the transfer of atoms across the interface (approximately equal to the activation energy for diffusion of Mo when the nucleus is coherent), k is the Boltzmann constant, h is the Planck constant,[24] and G^* is the activation energy for nucleation

$$G^* = \frac{16\pi}{3}\frac{\sigma^3}{\Delta G_V^2} \quad . \quad . \quad . \quad . \quad . \quad . \quad . \quad . \quad . \quad . \quad (14)$$

where ΔG_V is the chemical free energy change per unit volume of nuclei and has a negative value. Each critical sized embryo can be made supercritical by transferring an atom in contact with the embryo into it; it then becomes a nucleus. The nucleus size is represented as

$$r^* = -2\sigma/\Delta G_V \quad . \quad . \quad . \quad . \quad . \quad . \quad . \quad . \quad . \quad . \quad (15)$$

ΔG_V is calculated using MTDATA as $-1{\cdot}435 \times 10^9$ J m^{-3}. This value is for the beginning of precipitation of Mo_2C and it decreases as the precipitation proceeds. The change of the value of ΔG_V is calculated corresponding to the progress of the precipitation reaction using a mean field approximation, i.e. assuming that the solute is distributed uniformly in the matrix.

Diffusion controlled growth with capillarity

Modelling of growth with local equilibrium at the interface is based on Coates' diffusion controlled growth theory[11] accounting for the capillarity effect. The critical radius of curvature r_c at which growth ceases was calculated using MTDATA, with a modification to the database of the hcp phase to include a pressure change. The growth rate is the maximum rate obtained using Trivedi's theory, for given values of the carbon concentration in the matrix and the supersaturation Ω of Mo. The growth rate obtained from the values of $\bar{p}$ and the ratio r^{IC}/r_c corresponding to the maximum growth rate satisfies equation (1).

Ostwald ripening of particles

Coarsening occurs because the total energy of the system is reduced by eliminating interfaces; in practice, large particles grow more rapidly than small particles during precipitation, and large particles grow at the expense of smaller ones during classical coarsening. The average particle size therefore increases with time. Classical coarsening occurs slowly because of the small energies associated with the interfaces compared with the free energy change accompanying precipitation. Ostwald ripening can therefore be assumed to occur after the 'completion' of the precipitation of Mo_2C.

The combination of nucleation and growth described in the earlier part of this paper gives rise to a distribution of Mo_2C lengths, but for a given supersaturation, they all have the same tip radius. An approximate treatment is therefore adopted in which coarsening at first involves the spheroidisation of the needles assuming that the interfacial energy is isotropic. The spheroidisation is driven by the fact that the curvature at the plate tip is greater than on the sides of the needle. A Mo_2C particle is effectively modelled for coarsening purposes to be a cylinder with hemispherical ends. Particle growth and dissolution is then driven by the capillarity effect. The equilibrium concentration $c^{\alpha Mo_2C}_{Mo,r}$ at the hemispherical tip is given by

$$c^{\alpha Mo_2C}_{Mo,r} = (1 + 2\Gamma/r^{IC})c^{\alpha Mo_2C}_{Mo} \quad . \quad . \quad . \quad . \quad . \quad . \quad . \quad (16)$$

and $c^{\alpha Mo_2C}_{Mo,r}$ for a cylindrical body is given by

$$c^{\alpha Mo_2C}_{Mo,r} = (1 + \Gamma/r^{IC})c^{\alpha Mo_2C}_{Mo} \quad . \quad . \quad . \quad . \quad . \quad . \quad . \quad (17)$$

where Γ is the capillarity coefficient.

The concentrations of Mo were therefore calculated separately for the needle tip and body according to the respective curvatures. The growth or dissolution rates at the

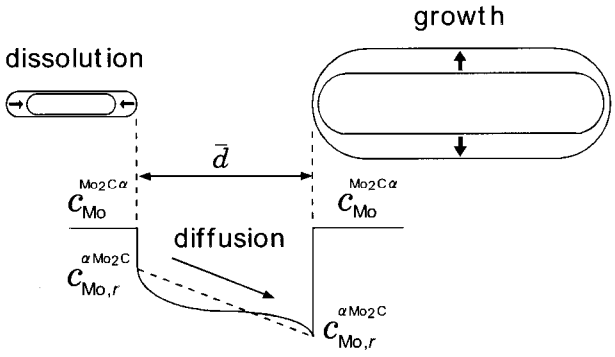

7 Schematic drawing of Ostwald ripening of cylinder shaped particles

tip and body were calculated for each particle using these concentrations, by the following equation

$$v = \frac{\bar{c}_{Mo} - c_{Mo,r}^{\alpha Mo_2C}}{c_{Mo}^{Mo_2C\alpha} - c_{Mo,r}^{\alpha Mo_2C}} \frac{D}{\bar{d}} \quad \ldots \quad (18)$$

where $\bar{d}$ is the mean diffusion distance between particles which can be represented as[23]

$$\bar{d} = (N^{\beta})^{-1/3} \quad \ldots \quad (19)$$

where N^{β} is the number density of Mo_2C particles. Accordingly, particles grow or dissolve as shown in Fig. 7.

Inputs and calculations

The precipitation calculations were done in steps of 100 s, and in each step, the nucleation rate, nucleus size which was the initial size of particle growth, growth rate, the Mo and C concentration change in the matrix corresponding to the growth of Mo_2C, and the enrichment and dissolution of cementite were calculated. The consumption of nucleation sites during the transformation was accounted for in each step. Once the concentrations of Mo and C in the matrix ($\bar{c}_{Mo}$ and $\bar{c}_C$) were determined, the corresponding supersaturation of Mo Ω_{Mo} and the critical radius r_c were obtained. If Ω_{Mo} and r_c were obtained, the value of $\bar{p}$ which satisfies equation (1), and finally, the maximum growth rate and the tip radius of a Mo_2C particle r^{IC} which gave the maximum rate for the corresponding value of $\bar{p}$ were obtained. The volume of each particle was calculated as a paraboloid.

After the completion of the precipitation and growth stage, each Mo_2C particle was modelled to be a needle of which both ends are hemispheres for the Ostwald ripening stage. In this stage, $c_{Mo,r}^{\alpha Mo_2C}$ at the tip and the body of each needle shaped particle were calculated, and then the growth (or dissolution) rates at the tip and the body were calculated.

The parameters used in the calculations are listed in Table 1. The nucleation site density was obtained by fitting with experimental data. The Mo_2C/ferrite interface energy,[20] and the diffusivity of molybdenum in ferrite[25] were obtained from the literature.

Results

Figure 8 shows the comparisons of the calculations and the experimental observations. Experimental data were obtained from several areas in each specimen. In Fig. 8, the solid circles represent the average of data from different areas, and the scatter of the data is indicated by an error bar. The technique allows the carbide dimensions to be measured to an accuracy of ± 1 nm.

After the completion of paraequilibrium cementite precipitation, the concentration of carbon in the matrix is quite low (0·026 at.-%, according to MTDATA). Carbon atoms, which are necessary for the precipitation of Mo_2C, are provided by the dissolution of cementite. After the completion of precipitation, Ostwald ripening proceeds with the constant volume fraction of Mo_2C. Figure 8*a* shows such simultaneous Mo_2C precipitation and cementite dissolution behaviour. From the observations and calculations, the volume fraction of Mo_2C increases with time up to 100 h and then remains constant, as shown in Fig. 8*a*. It is therefore considered that nucleation and growth stage ends at $\sim$100 h and the Ostwald ripening stage commences after that.

The average length of Mo_2C particles increases during the precipitation and growth stage. During the Ostwald ripening stage the growth rate (or dissolution rate) at the both ends of a needle is smaller (or larger) than that at the body of a needle because of the capillarity effect. As an average, the length therefore decrease during Ostwald ripening as shown in Fig. 8*b*.

The number density of Mo_2C particles with length greater than 5 nm was calculated, as shown in Fig. 8*c*, for comparison with observations; Mo_2C particles of size less than 5 nm could not easily be observed using conventional TEM. During the Ostwald ripening stage, the number density decreases.

The calculated number density distribution of the length of Mo_2C particles is shown in Fig. 8*d* for the tempering time of 30 h. Each point which is placed at the length of X nm represents the number density of the observed particles whose length is from $(X-5)$ nm to $(X+5)$ nm.

Discussion

The calculations in general agree well with the observations. However, there are discrepancies in the number density of Mo_2C, and the number density distribution of the length of Mo_2C particles. The problem probably lies in the evaluation of nucleation rate. The observations show that even after 100 h tempering, small particles (10–20 nm) exist whereas the calculations show that nucleation ceases in the relatively early stages of tempering. Nucleation is considered to occur more slowly and consistently than implied by the calculations until a relatively late stage of tempering. It is not clear how the nucleation function should be adapted without introducing further unknown parameters such as strain energy.

In the present model, cementite is modelled as a plate although in practice its morphology is not uniform. To test this assumption, another calculation in which cementite is

Table 1 Calculation parameters for precipitation of carbides in ternary system (Fe–0·1 wt-%C–1·6 wt-%Mo)

Parameter	Condition
Shape of Mo_2C	Needle
Tempering temperature, °C	600
Interface energy of Mo_2C, J m^{-2}	0·2
Driving force for nucleation of Mo_2C, J m^{-3}	$-1{\cdot}435\times10^{9}$
Nucleation site density of Mo_2C, m^{-3}	$2{\cdot}46\times10^{22}$
Maximum volume fraction of cementite	$1{\cdot}796\times10^{-2}$
Maximum volume fraction of Mo_2C	$1{\cdot}391\times10^{-2}$
Atomic fraction $c^{\alpha\theta}$	$8{\cdot}724\times10^{-3}$
Atomic fraction $c^{\beta\alpha}$	$4{\cdot}245\times10^{-2}$
Atomic fraction $c^{\alpha Mo_2C}$	$1{\cdot}632\times10^{-3}$
Atomic fraction $c^{Mo_2C\alpha}$	$6{\cdot}556\times10^{-1}$
Thickness of cementite in grains, m	$2{\cdot}0\times10^{-8}$
Thickness of cementite on grain boundaries, m	$5{\cdot}0\times10^{-8}$
Diffusion constant of Mo D_{Mo}, m^2 s^{-1}	$2{\cdot}29\times10^{-4}$
Activation energy for Mo diffusion Q_{Mo}, J mol^{-1}	$2{\cdot}39\times10^{5}$

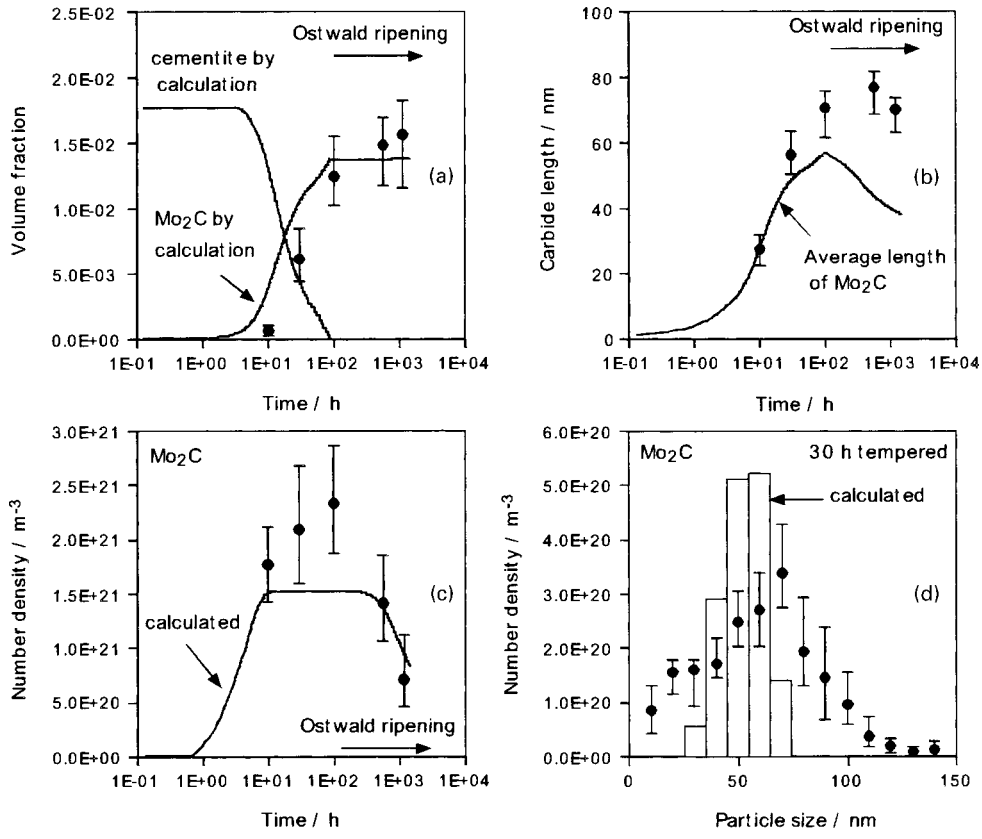

a relationship between volume fraction of Mo_2C particles and tempering time; *b* relationship between average length of Mo_2C particles and tempering time; *c* relationship between number density of Mo_2C particles whose size are over 5 nm and tempering time; *d* number density distribution of length of Mo_2C particles for 30 h tempered specimen

8 Comparisons between calculations and observations

modelled as spheres and the capillarity effect is taken into account was carried out. This predicted that cementite dissolution is completed 6 h earlier than in the present model. It is therefore considered that although the detailed morphology of the cementite should affect its dissolution, the difference in time is relatively small compared with that for the alloy carbide reaction.

The growth model used here is based on Trivedi's theory where the needle is represented as a paraboloid of revolution. For comparison, a calculation based on Zener's approximation, as adopted by Fujita and Bhadeshia,[3] was performed. Even by varying the nucleation site density, it was impossible to fit the results to observations. In particular, the model overestimates the growth rate, as shown in Fig. 9.

For the Ostwald ripening stage, Mo_2C particles was modelled as a needle with hemispherical ends. Coarsening theory for spheres leads to the following relationship[26,27]

$$r^3 - r_0^3 = \left(\frac{8\sigma v^{\beta} D_{Mo} c_{Mo}^{\alpha\beta}}{9kT} \right) t \quad \ldots\ldots\ldots \quad (20)$$

where r is the average radius, r_0 is the initial average particle radius and t is time. During Ostwald ripening, the volume fraction of Mo_2C can be assumed to be constant. The number density of Mo_2C can be therefore represented as

$$N^{Mo_2C} = N_0^{Mo_2C} r_0^3 \Big/ \left(r_0^3 + \frac{8\sigma v^{\beta} D_{Mo} c_{Mo}^{\alpha\beta}}{9kT} t \right) \quad \ldots \quad (21)$$

where $N_0^{Mo_2C}$ is the initial number density of Mo_2C precipitates when the Ostwald ripening stage starts.

Figure 10 shows comparisons of the transition of $N_0^{Mo_2C}$ during Ostwald ripening calculated as needle, as sphere and by equation (21). The calculation as needle is identical for the Ostwald ripening stage of Fig. 8*c*. The calculations as needle and sphere get similar results, and show the similar tendency the result of equation (21).

Summary and conclusions

The precipitation and Ostwald ripening behaviour of Mo_2C (needle shaped) particles during the tempering of a ternary

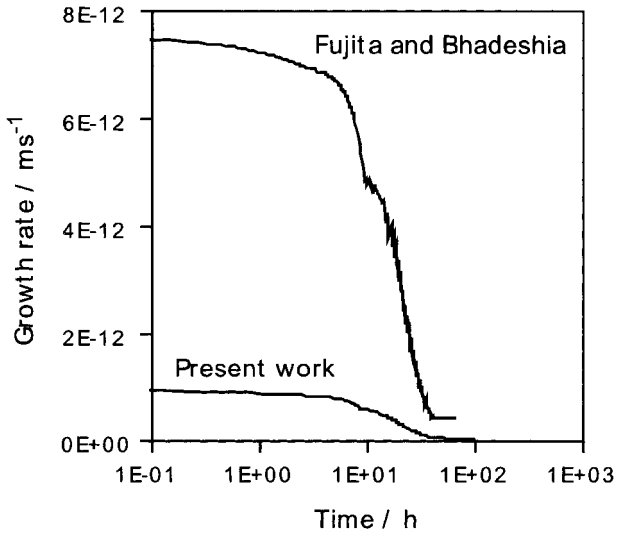

9 Comparisons of growth rate of Mo_2C particles between Fujita and Bhadeshia model[3] and present model

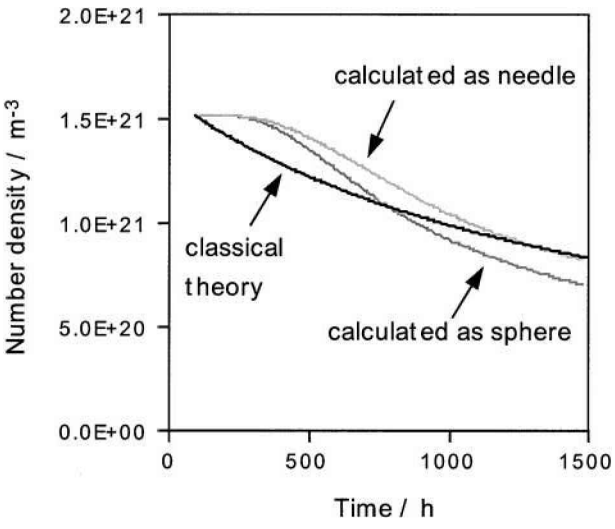

10 Comparisons of number density of Mo_2C particles calculated as needle shaped, spherical and by equation (21)

Fe–C–Mo martensitic steel have been characterised and modelled, taking account of local equilibrium, the capillarity effect, and simultaneous cementite enrichment and dissolution.

In conclusion, by modelling a Mo_2C particle as a paraboloid and assuming the maximum growth rate, the model has been shown to be capable of estimating the average length, volume fraction, and number density of particles in a manner consistent with experimental observations. The growth rate depends on the supersaturation of Mo Ω^{M_o} and the ratio of the solute concentration in the matrix $\bar{c}_{M_o}/\bar{c}_C$.

Acknowledgements

The authors are grateful to the Nippon Steel Corp. for funding this research, to Professor D. J. Fray for the provision of laboratory facilities at the University of Cambridge and to Vicky Yardley for many helpful comments on the draft manuscript.

References

1. N. IBARAKI, A. INADA, M. SHIMOTSUSA, T. NAKAYAMA, T. IWATA and M. NAGAO: *Kobelco Technol. Rev.*, 1998, **21**, 21–25.
2. T. KUSHIDA, N. KURATOMI, T. KUDOH, H. MATSUMOTO, T. TSUMURA and F. NAKASATO: *Tetsu-to-Hagane (J. Iron Steel Inst. Jpn)*, 1996, **82**, 297–302.
3. N. FUJITA and H. K. D. H. BHADESHIA: *Mater. Sci. Technol.*, 1999, **15**, 627–334.
4. C. ZENER: *Trans. AIME*, 1946, **167**, 550–595.
5. R. TRIVEDI: *Acta Metall.*, 1970, **18**, 287–295.
6. A. HULTGREN: *Trans. ASM*, 1968, **39**, 915–1005.
7. H. K. D. H. BHADESHIA: 'Bainite in steels', 2nd edn, 63; 2001, London, IoM Communications.
8. S. S. BABU, K. HONO and T. SAKURAI: *Appl. Surf. Sci.*, 1993, **67**, 321–327.
9. R. C. THOMSON and M. K. MILLER: *Appl. Surf. Sci.*, 1995, **87–88**, 185–193.
10. R. C. THOMSON and M. K. MILLER: *Acta Metall.*, 1998, **46**, 2203–2213.
11. D. E. COATES: *Metall. Trans.*, 1972, **3**, 1203–1212.
12. G. P. IVANTSOV: *Dolk. Akad. Nauk. SSSR*, 1947, **58**, 567–569.
13. G. HORVAY and J. W. CAHN: *Acta Metall.*, 1961, **9**, 695–705.
14. M. ABRAMOWITZ: 'Hand book of mathematical functions', 228; 1965, New York, NY, Wiley.
15. R. TRIVEDI: *Metall. Trans.*, 1970, **1**, 921–927.
16. P. E. J. RIVERA and H. K. D. H. BHADESHIA: *Mater. Sci. Technol.*, 2001, **17**, 25–29.
17. P. M. KELLY and J. NUTTING: *J. Iron Steel Inst.*, 1959, **192**, 246–248.
18. R. T. DEHOFF: 'Thermodynamics in materials science', 378; 1993, New York, McGraw–Hill.
19. S. M. HODSON: 'MTDATA – metallurgical and thermochemical databank'; 1989, Teddington, National Physical Laboratory.
20. D. A. PORTER and K. E. EASTERLING: 'Phase transformations and alloys', 2nd edn, 147; 1992, London, Chapman and Hall.
21. M. TAKAHASHI and H. K. D. H. BHADESHIA: *Mater. Sci. Technol.*, 1990, **6**, 592–603.
22. H. K. D. H. BHADESHIA: *Mater. Sci. Technol.*, 1989, **5**, 131–137.
23. J. D. ROBSON and H. K. D. H. BHADESHIA: *Mater. Sci. Technol.*, 1997, **13**, 631–639.
24. J. W. CHRISTIAN: 'The theory of transformations in metals and alloys', 2nd edn, Part 1, 441; 1975, Oxford, Pergamon Press.
25. P. HEIJWEGEN and G. D. RIECK: *Acta Metall.*, 1974, **22**, 1268–1281.
26. M. LIFSHITZ and V. V. SLYOZOV: *J. Phys. Chem. Solids*, 1961, **19**, 35–50.
27. R. WARGNER and R. KAMPMANN: 'Materials science technology', Vol. 5, 213–303; 1991, Weinheim, VCH.